ELSEVIER

Chemical Geology 244 (2007) 715–729

CHEMICAL GEOLOGY
INCLUDING
ISOTOPE GEOSCIENCE

www.elsevier.com/locate/chemgeo

Time series δ^{26}Mg analysis in speleothem calcite: Kinetic versus equilibrium fractionation, comparison with other proxies and implications for palaeoclimate research

D. Buhl [a], A. Immenhauser [a,*], G. Smeulders [b], L. Kabiri [c], D.K. Richter [a]

[a] *Ruhr-Universität Bochum, Institute for Geology, Mineralogy and Geophysics, Universitätsstrasse 150, D-44801 Bochum, Germany*
[b] *Vrije Universiteit Amsterdam, Faculty of Earth and Life Sciences, De Boelelaan 1085, 1081 HV Amsterdam, The Netherlands*
[c] *Laboratoire des Formations Superficielles: Science du Climat, de l'Eau, de l'Environnement et du Patrimoine [LFS/SCEEP], Département de Géologie, Faculté des Sciences et Techniques Er Rachidia [FSTE], BP 509 Boutalamine 52 000 Er Rachidia, Morroco*

Received 15 November 2006; received in revised form 6 July 2007; accepted 22 July 2007

Editor: S.L. Goldstein

Abstract

Magnesium-isotope time series MC-ICP-MS analyses from a Pleistocene speleothem – collected in a limestone cave in NW Africa (Morocco) – are reported and discussed in a process-oriented context. In addition, high-resolution C, O and Sr-isotope data, and Mg and Sr element abundances were compiled from the same stalagmite. Sub-samples were collected along the stalagmite growth axis and a second data set was drilled perpendicularly within one growth interval (Hendy test). The analytical results show clearly co-variant, systematic and cyclical fluctuations for all proxies collected along the growth axis and – with respect to the analytical error – invariant data within one growth increment. Magnesium-isotope ratios (δ^{26}Mg) fluctuate between −4.39‰±0.02 2σ and −4.17‰±0.05 2σ and are within the range of published results of speleothem calcite from limestone caves. The difference of 0.22‰ is significantly beyond the error of the external reproducibility of ±0.03‰ 2σ for δ^{26} Mg. Considering the analytical error, neither a purely kinetic nor an equilibrium fractionation process explains the observed isotope pattern. For the time being, it is suggested that two external factors drive the speleothem Mg-isotope cyclicity: (1) climate-driven (arid versus humid) variances in the precipitation rate of a carbonate phase from meteoric water within the karstic system prior to entering the cave system; and (2) changing rates of silicate (aeolian material) versus carbonate weathering. Both of these processes fractionate the Mg-isotopic composition of runoff/seepage water. There is evidence that the magnesium-isotope system, applied to speleothem archives, bears significant information concerning continental climatic variability in arid zones and deserves further research.

Keywords: Magnesium isotopes; Speleothems; Kinetic fractionation; Equilibrium fractionation; Climate proxy

1. Introduction

Variations in the $^{18}O/^{16}O$ and $^{13}C/^{12}C$ ratios and trace element compositions in calcite speleothems can provide concise and well-dated information about terrestrial palaeoclimate (e.g., Hendy, 1971; Huang et al., 2001;

* Corresponding author. Tel.: +49 234 32 28250; fax: +49 234 32 14571.
E-mail address: adrian.immenhauser@rub.de (A. Immenhauser).

0009-2541/$ - see front matter © 2007 Elsevier B.V. All rights reserved.
doi:10.1016/j.chemgeo.2007.07.019

Spötl et al., 2002; Fleitmann et al., 2003a). These geochemical variations are determined by the environmental conditions at the time of deposition and by kinetic and equilibrium fractionation processes during precipitation (White, 2004). In contrast, magnesium-isotopes (Chang et al., 2004; Young and Galy, 2004) of continental systems (de Villiers et al., 2005; Tipper et al., 2006b) and particularly of speleothem calcite (Galy et al., 2002) have yet received little attention. This is mainly due to the more complex analytical processes involved. State-of-the-art multi-collector inductively coupled plasma mass spectrometry (MC-ICP-MS), however, makes the analysis of these non-conventional isotope systems feasible and provides sufficient precision to resolve significant differences in these climatic archives.

Here we report on time-series Mg-isotope data from a Middle to Lower Pleistocene (>500 ka) low-Mg calcite speleothem, collected in a cave near Er Rachidia (Anti-Atlas, Morocco; Fig. 1) and relate the analytical results to $\delta^{13}C$, $\delta^{18}O$, $^{87}Sr/^{86}Sr$ as well as Sr and Mg element data (Table 1). Previous authors (Galy et al., 2002) reported individual data of various speleothems and drip water from caves in the Alps and Israel and suggested a strong mineralogical control and a weak temperature effect on the Mg-isotope ratios of spelean calcite (Table 2). Galy et al. (2002), however, documented only a very limited data set for temporal variations of Mg isotopes within specific, limestone hostrock speleothems with most data shown originating from dolostone hostrock caves. Here a higher resolution time-series data set from a limestone hostrock cave sampled along the growth axis and a second data set sampled within a growth increment perpendicular to the main growth axis are presented (Fig. 2).

The aims of this paper are threefold: firstly, high-resolution time-series and time-parallel speleothem Mg-isotope data are presented and discussed in a process-oriented context; secondly, the correlation of the speleothem Mg, C, O and Sr-isotope record and the Sr and Mg element composition is assessed; thirdly, controlling factors of Mg-isotope fractionation in spelean calcite are discussed and particularly the significance of kinetic versus equilibrium fractionation. The data presented here are significant as Mg has the

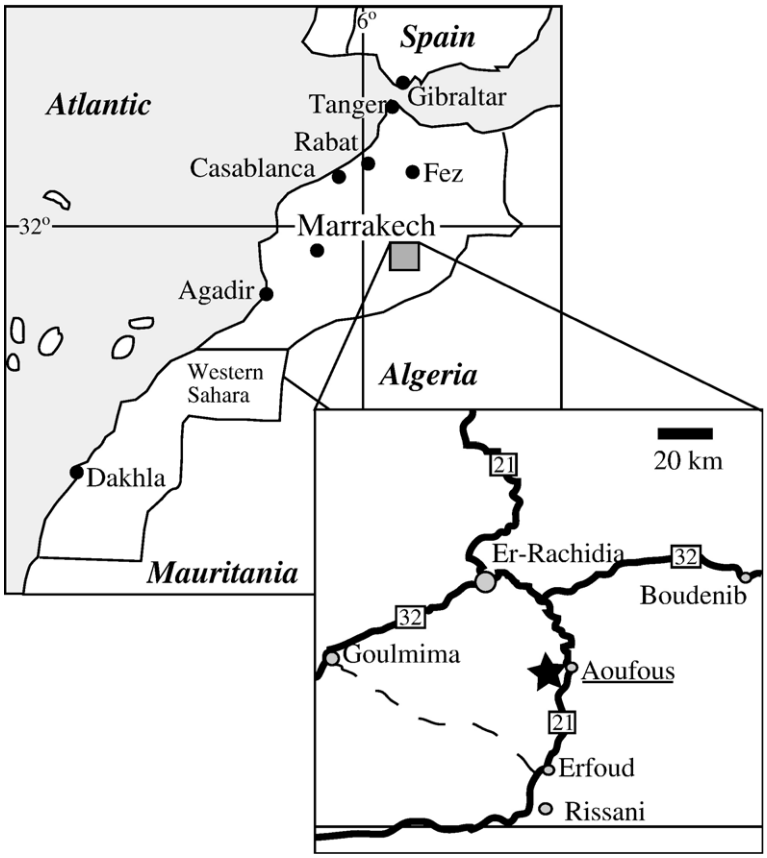

Fig. 1. Overview map of Morocco. Lower right inset map shows locality of Aoufous cave in the Anti-Atlas area (asterisk).

Table 1
Results of time series analyses (along growth axis) of trace elements and stable isotopes of the Aoufous stalagmite and Turonian host-rock

Sample number	Mg ppm	Sr ppm	Fe ppm	δ^{13}C‰ (VPDB)	δ^{18}O‰ (VPDB)
V001	nd	710	136	−0.4	−9.4
V002	nd	680	nd	−0.2	−9.3
V003	7565	602	255	+0.3	−9.6
V004	5074	390	17	+1.1	−10.0
V005	3706	281	272	+1.5	−9.7
V006	3945	309	211	+0.9	−10.0
V007	3712	271	207	+0.7	−10.2
V008	3317	265	18	+0.2	−10.5
V009	2999	217	54	+0.6	−10.2
V010	3041	234	111	+0.3	−10.6
V011	4302	455	41	−3.9	−10.5
V012	7225	583	10	−5.5	−10.5
V013	7271	487	50	−5.7	−10.8
V014	nd	542	86	−5.9	−10.9
V015	7021	496	54	−5.3	−10.4
V016	7099	531	540	−5.5	−11.2
V017	nd	454	101	−5.7	−10.9
V018	8034	445	211	−6.0	−11.1
V019	8022	485	152	−5.9	−11.3
V020	8171	528	79	−5.9	−11.3
V021	nd	505	nd	−5.6	−10.9
V022	7201	567	811	−5.4	−10.8
V023	7044	576	1124	−5.0	−11.2
V024	nd	554	26	−5.7	−11.0
V025	7400	620	22	−4.8	−11.1
V026	7653	486	23	−6.2	−10.9
V027	7434	439	52	−6.3	−10.6
V028	7446	430	115	−6.3	−10.8
V029	nd	459	17	−5.8	−11.1
V030	7180	529	nd	−5.1	−11.0
V031	7291	519	nd	−4.8	−10.7
V032	nd	546	nd	−4.4	−10.8
V033	7161	537	nd	−3.9	−10.8
V034	6625	524	46	−3.7	−10.8
V035	nd	585	49	−4.3	−9.9
V036	7762	567	29	−4.1	−10.1
V037	nd	473	13	−4.2	−9.9
V038	nd	nd	nd	−4.3	−9.9
V039	7922	607	nd	−4.3	−11.0
V040	8035	nd	nd	−4.7	−11.8
V041	8053	654	64	−4.7	−11.8
V042	8254	nd	nd	−5.1	−12.4
V043	nd	660	nd	−4.4	−11.5
V044	8361	nd	nd	−4.0	−10.6
V045	nd	700	nd	−4.5	−10.6
V046	8402	nd	nd	−4.7	−10.9
V047	nd	689	nd	−4.9	−10.8
V048	8138	nd	nd	−4.9	−11.0
V049	8253	721	nd	−5.1	−10.8
V050	nd	nd	nd	−4.5	−10.8
V051	8493	834	35	−3.8	−10.2
V052	8501	nd	nd	−3.8	−10.2
V053	nd	824	nd	−4.3	−9.9
V054	nd	nd	nd	−3.8	−9.8
V055	8855	1011	nd	−3.2	−9.8
V056	8801	nd	nd	−2.6	−9.5
V057	8762	981	nd	−2.6	−9.4
V058	8541	nd	nd	−2.4	−9.4
V059	8319	967	nd	−2.4	−9.2
V060	8872	nd	nd	−2.2	−9.7
V061	8421	955	nd	−2.7	−10.1
V062	nd	nd	nd	−2.5	−9.9
V063	8644	994	nd	−2.4	−9.7
V064	8532	nd	nd	−2.5	−9.8
V065	nd	954	23	−2.3	−9.6
V066	8761	nd	nd	−2.5	−9.5
V067	8852	927	32	−2.2	−9.2
V068	nd	nd	nd	−2.1	−9.1
V069	nd	910	17	−2.2	−9.4
V070	nd	nd	nd	−2.1	−9.7
V071	nd	915	20	−2.0	−9.2
V072	nd	nd	nd	−2.0	−9.3
V073	9041	836	68	−2.6	−9.5
V074	9533	nd	nd	−2.6	−9.6
V075	9661	819	309	−2.8	−9.8
V076	nd	nd	nd	−2.8	−9.9
V077	8423	687	11	−3.3	−10.0
V078	8589	nd	nd	−3.3	−10.4
V079	nd	754	nd	−3.2	−10.7
V080	8633	nd	nd	−3.5	−10.7
V081	8789	853	10	−6.0	−11.5
V082	nd	nd	nd	−6.0	−11.3
V083	7862	824	1255	−6.2	−11.0
V084	nd	nd	nd	−6.2	−11.0
V085	7955	755	nd	−6.2	−11.1
V086	nd	nd	nd	−6.1	−10.8
V087	7844	737	133	−6.0	−10.4
V088	7536	nd	nd	−5.1	−10.2
V089	nd	645	nd	−5.1	−10.0
V090	7267	nd	nd	−5.3	−9.7
V091	7367	599	11	−5.4	−10.0
V092	7031	nd	nd	−5.3	−10.1
V093	nd	662	16	−4.0	−9.9
V094	6992	nd	nd	−2.8	−9.6
V095	6983	638	11	−4.5	−11.2
V096	nd	nd	nd	−5.6	−11.3
V097	5973	586	25	−5.8	−10.7
V098	5974	nd	nd	−4.4	−10.9
V099	5422	408	316	−4.8	−11.0
V100	nd	nd	nd	−2.0	−9.6
Max	9661	1011	1255	+1.5	−9.1
Min	2999	217	nd	−6.4	−12.4
Average	7393	617	110	−3.8	−10.4
Standard dev. 1σ	1581	198	233	1.9	0.7
Hostrock 1	4735	728	237	0.1	−7.5
Hostrock 2	nd	nd	nd	0.2	−7.6
Hostrock 3	4431	826	39	−0.9	−6.5
Hostrock 4	nd	nd	nd	−0.8	−6.6
Hostrock 5	4169	711	438	0.4	−7.0
Hostrock 6	nd	nd	nd	0.4	−7.1
Hostrock 7	4315	881	1902	1.7	−6.8
Hostrock 8	nd	nd	nd	1.8	−6.8

(continued on next page)

Table 1 (*continued*)

Sample number	Mg ppm	Sr ppm	Fe ppm	δ^{13}C‰ (VPDB)	δ^{18}O‰ (VPDB)
Hostrock 9	nd	nd	nd	0.1	−5.4
Hostrock 10	nd	nd	nd	0.2	−5.3
Hostrock 11	nd	nd	nd	0.4	−7.9
Hostrock 12	nd	nd	nd	0.5	−7.8
Max	4735	881	1902	1.8	5.3
Min	4169	711	39	−0.9	−7.5
Average	4413	787	654	0.3	−6.9
Standard dev. 1σ	240	81	848	0.8	0.8

nd indicates no data. Sample V001 is at base, sample V100 at top of speleothem.
Please note that trace element data are normalized to the Ca concentration of pure calcite (40 wt.%). Trace element data indicate geochemical trends.

potential to become an important additional climate proxy in speleothem research providing the controlling mechanisms are better understood.

2. Case setting and carbonate materials

The fossil, calcitic speleothem (stalagmite, 18 cm in length) chosen for this study was collected in a presently dry cave near Aoufous (south of Er-Rachidia) in the Anti-Atlas area of Morocco (Fig. 1). The cave is situated at an altitude of approximately 1000 m, the present-day annual precipitation rate ranges from 12 to 69 mm/year and the present-day average temperature range between 21 and 26 °C. The host rock is a non-metamorphic, Turonian, shallow-marine limestone (low-Mg calcite).

An attempt to date the age of the stalagmite using the U–Th approach indicated that it falls outside of the dating window of 500 kyr. For the time being, its age remains thus unspecified. Several other speleothems from the same cave were investigated too (U–Th) and all consistently suggested ages of older than 500 kyr. U–Pb age dating of some of these speleothems is presently under way. This pattern might be of significance for the climate history of NW Africa but is not the focus of the present paper.

The calcite is well preserved as indicated by its intrinsic cathode luminescence (CL; Fig. 3). The stalagmite is characterized by blue CL colours implying a low Mn content. Irregular, dark blue luminescent zones alternate with light blue ones. These colour shifts are due to irregularities in the calcite crystal lattice and fluctuating fluid inclusion density or pigmentation. The outer few mm of the stalagmite show evidence of corrosion and display a zoned image of blue and violet to orange colours (Fig. 3a). This is due to changing Mn contents under CL. This outer rim of the speleothem was

Table 2
Overview of Mg-isotope data from the Aoufous speleothem and the Turonian hostrock and data (*) from Galy et al. (2002)

Sample number	Fig. 2	Sample type	δ^{25} Mg [‰DSM3]	±2σ	δ^{26} Mg [‰DSM3]	±2σ	δ^{25} Mg′ [‰DSM3]	±2σ	δ^{26} Mg′ [‰DSM3]	±2σ
Pos 3/4	1	Speleothem	−2.22	0.03	−4.28	0.04	−2.22	0.03	−4.29	0.04
Pos 5	2	Speleothem	−2.24	0.02	−4.33	0.04	−2.25	0.02	−4.34	0.04
Pos 10	3	Speleothem	−2.28	0.02	−4.38	0.05	−2.28	0.02	−4.39	0.05
Pos 14/15	4	Speleothem	−2.26	0.02	−4.35	0.05	−2.26	0.02	−4.36	0.05
Pos 17	5	Speleothem	−2.27	0.02	−4.39	0.02	−2.28	0.02	−4.40	0.02
Pos 20	6	Speleothem	−2.23	0.03	−4.26	0.04	−2.23	0.03	−4.27	0.04
Pos 22a	7	Speleothem	−2.19	0.02	−4.23	0.03	−2.19	0.02	−4.23	0.03
Pos 25	8	Speleothem	−2.21	0.02	−4.26	0.04	−2.21	0.02	−4.27	0.04
Pos 30	9	Speleothem	−2.17	0.01	−4.17	0.05	−2.17	0.01	−4.17	0.05
Pos 37	10	Speleothem	−2.20	0.02	−4.23	0.06	−2.20	0.02	−4.24	0.06
Pos 40	11	Speleothem	−2.16	0.02	−4.18	0.03	−2.17	0.02	−4.19	0.03
Pos 45	12	Speleothem	−2.25	0.02	−4.31	0.08	−2.25	0.02	−4.32	0.08
Pos 33a	13	Speleothem	−2.19	0.01	−4.22	0.01	−2.19	0.01	−4.23	0.01
Pos 33b	14	Speleothem	−2.18	0.01	−4.20	0.03	−2.19	0.01	−4.21	0.03
Pos 33c	15	Speleothem	−2.18	0.02	−4.19	0.04	−2.18	0.02	−4.20	0.04
Pos 33d	16	Speleothem	−2.18	0.03	−4.21	0.03	−2.19	0.03	−4.21	0.03
Pos 33e	17	Speleothem	−2.17	0.02	−4.19	0.03	−2.17	0.02	−4.20	0.03
Pos 33f	18	Speleothem	−2.19	0.01	−4.22	0.02	−2.19	0.01	−4.23	0.02
TurA		Hostrock	−1.86	0.04	−3.57	0.09	−1.86	0.04	−3.58	0.09
TurB		Hostrock	−1.93	0.03	−3.69	0.07	−1.94	0.03	−3.70	0.07
PEK-6-A*		Speleothem	−1.48	0.01	−2.80	0.09	−1.48	0.01	−2.80	0.09
PEK-9-A*		Speleothem	−2.24	0.02	−4.32	0.02	−2.24	0.02	−4.33	0.02
PEK-9-C*		Speleothem	−2.25	0.03	−4.39	0.08	−2.25	0.03	−4.40	0.08
PEK-9-D*		Speleothem	−2.22	0.04	−4.32	0.04	−2.22	0.04	−4.33	0.04
TDGW*		drip water	−1.27	0.05	−2.42	0.12	−1.27	0.05	−2.42	0.12
TDGS*		Speleothem	−2.63	0.05	−5.09	0.07	−2.63	0.05	−5.10	0.07

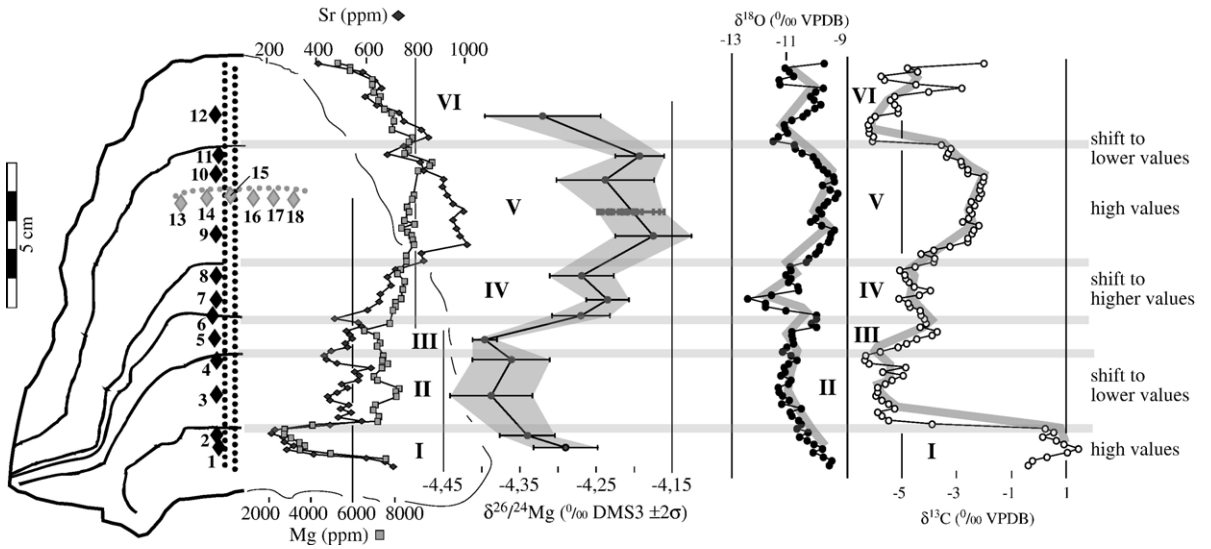

Fig. 2. Overview of geochemical data from the Aoufous speleothem. Outline of cut and polished slab is shown and left side highlighted. Black dots on speleothem indicate sampling points for stable isotopes and trace elements along the growth axis; gray dots indicate sampling localities within one growth increment (Hendy test); black and gray diamonds indicate sampling points for δ^{26}Mg analyses. Sampling numbers 1 to 18 refer to isotope data in Table 2. Grey horizontal bars represent hiatuses within the stalagmite. Gray lines underlying carbon and oxygen plots represent 5-point moving average. Note the overall broad co-variance of most data sets overprinted by smaller order, punctuated events for instance across hiatuses. Tentative growth segments of the speleothem, representing different growth intervals (separated by hiatuses), are labelled I to VI.

not sampled for geochemical analysis. The outcome of this CL study is clear evidence of a well preserved, i.e., non-altered, calcitic speleothem (Richter et al., 2002) forming a suitable carbonate material for the assessment of the time-series Mg-isotope data set. The $MgCO_3$ content of the speleothem is 3 mol% (low-Mg calcite with elevated Mg content) as indicated by XRF analysis using quartz powder as an internal standard. Drip-water data could not be measured as the water has ceased to flow under the increasingly arid climates of NW Africa.

Petrographic analysis reveals that the speleothem calcite is characterized by a fibrous to elongate crystal fabric with crystal length:width ratios of more than 6:1 (see discussion in Frisia et al., 2000). The calcite crystals show undulous extinction and slightly converging crystal axes (dip is 0.3 to 0.9° per 100 μm crystal width), an observation that is well in agreement with its elevated Mg content (Neuser and Richter, 2007).

3. Analytical methods

Twelve samples for Mg-isotope analysis were extracted along the growth axis (black diamonds 1-11 in Fig. 2) and six were drilled along an individual growth increment (gray diamonds 12–17 in Fig. 2) using a micro drilling system (MicroMill, Mechantek; Dettman and Lohman, 1995). Approximately 3 mg of rock powder was extracted from 1*1*1 mm (1 mm^3) sized pits drilled into the polished surface of the slab and was recovered using a 1 μl pipette and ultra pure water. The samples were dissolved in 6 M HCl (supra pure). Subsequently the solution was dried and 100 to 200 μl of $HClO_4$ were added to destroy organic compounds, minimizing possible interferences related to complexing of cations. The solution was evaporated until dryness and the samples were re-dissolved applying HCl 2.5 M. The Mg fraction was recovered using BioRad ion exchange resin AG50 W-X12 (200 to 400 mesh) and quartz glass columns. A 500 ppb Mg-solution in 3.5% HNO_3 was measured on a ThermoElectron Neptune MC-ICP-MS in the isotope laboratory of the Ruhr-Universität Bochum, Germany. The difference between the Mg concentration of the standard and sample was kept within a 25% limit, which proved to minimize potential isobaric interferences from matrices (Galy et al., 2001).

A positive effect on signal stability and reduction of matrix interferences was achieved by a combination of two desolvating systems (ApexIR (ESI) and Aridus (Cetac)). A 500 ppb Mg DSM3 standard solution was aspirated, which resulted in 19 V (10^{11} Ω resistor) for the mass ^{24}Mg. The signal intensities of samples ranged between 18 V and 20 V for mass ^{24}Mg.

The bracketing standard technique was applied to calculate the δ^{25}Mg and δ^{26}Mg values. All δ-values

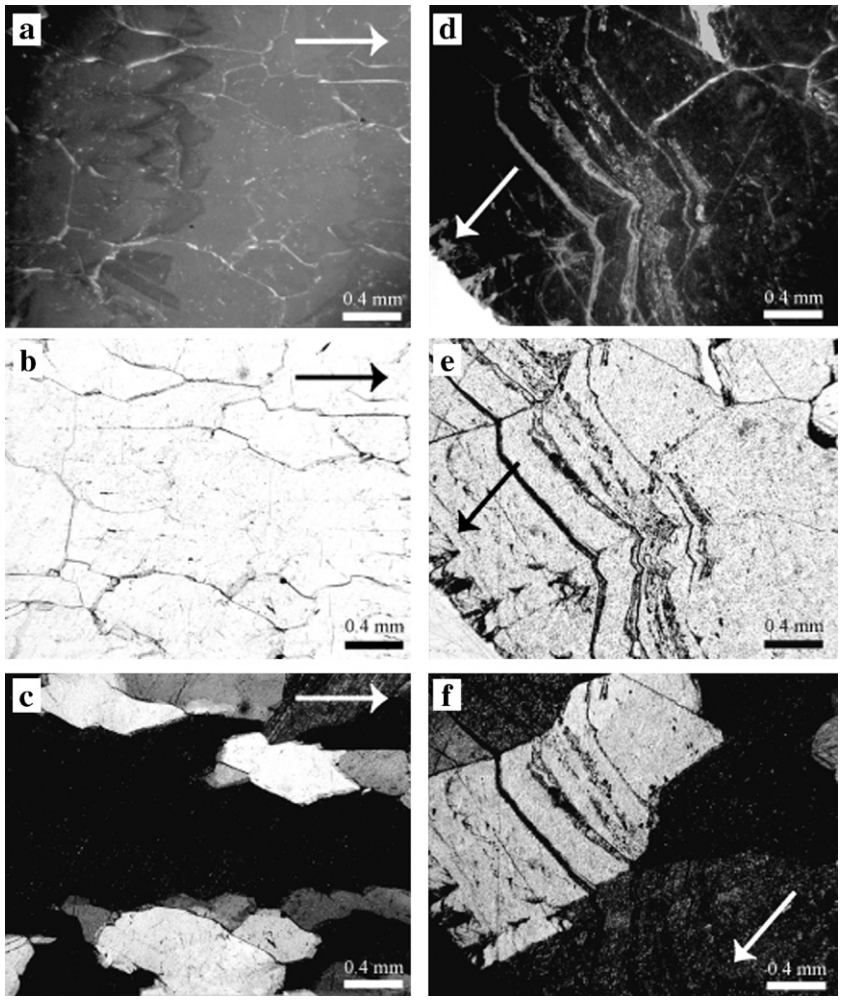

Fig. 3. Thin section images of the Aoufous speleothem. Images a–c show central part of speleothem (growth direction indicated by arrow). Images d–f show marginal part of speleothem (growth direction indicated by arrow). Images a–d = cathode luminescence; b–e = normal light; c–f = crossed nicols. Intrinsic luminescence with minor variations is indicative of free crystal growth (thick water film). Marginal zones characterized by Mn^{2+}-rich calcite (orange luminescence). Laminae might be indicative of inhibited crystal growth and thin water film.

presented in this study are based on a sequence of 5 repetitions measured from the same solution, representing the internal precision of measurements (2σ-errors). The external precision was tested with 6 samples from the same layer ("Hendy test"; Hendy, 1971, gray diamonds in Fig. 2) that underwent the complete sampling, chemical separation and measurement procedure. The mean value for the δ^{26}Mg and δ^{25}Mg are $-4.205‰ \pm 0.030$ 2σ and $-2.181‰ \pm 0.13$ 2σ, respectively. As SRM the DSM3 was chosen because of the published Mg-isotope heterogeneity of the NBS980 (Galy et al., 2003; Table 3). The source of the DSM3 is pure Mg metal provided by Dead Sea Magnesium Ltd. The 500 ppb working standard solution bases on an aliquot

Table 3
Comparison of different standards

Standard	δ^{26}Mg	δ^{25}Mg	Number of analyses
SRM980 (Oxford) vs. DSM3	−3.40±0.13‰	−1.74±0.07‰	n=10
SRM980 (Bochum) vs. DSM3	−4.49±0.18‰	−2.31±0.04‰	n=85
Cambridge1 (Oxford) vs. DSM3	−2.58±0.14‰	−1.33±0.07‰	n=35
Cambridge1 (Bochum) vs. DSM3	−2.56±0.06‰	−1.33±0.03‰	n=250

Compilation of data over a period of nine months, all errors are 2σ errors.

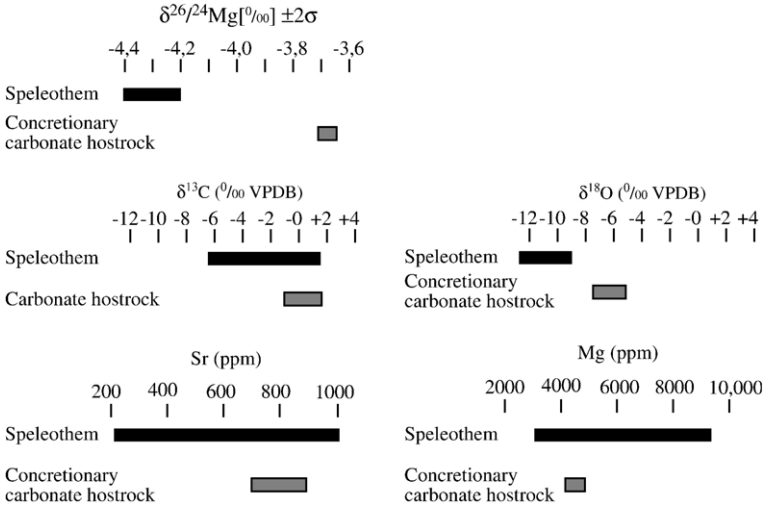

Fig. 4. Comparison of speleothem and hostrock geochemical composition. Black bars indicate speleothem data and gray bars indicate Turonian concretionary host limestone data.

of a stock solution DSM3 (10,000 ppm) distributed by Albert Galy, Cambridge, UK. The reproducibility of the standard measurements is tested against a second solution kindly provided by Galy, the Cambridge1. For the year 2006 the mean values for Cambridge1 are δ^{25}Mg= −1.325‰ DSM3±0.031 2σ and δ^{26} Mg=−2.558‰ DSM3±0.062 2σ (n=45), respectively. The average out of 13 measurements of DSM3 vs. Cambridge1, performed in June 2006 is δ^{25}Mg=−1.313‰ DSM3±0.030 2σ and δ^{26}Mg=−2.561‰ DSM3±0,060 2σ.

A progressive coating of the cones over a period of a couple of days causing an increase of the Mg background could be dealt with by frequent cleaning of the cones. On average the background signal for the mass 24 was below 10 mV (R10[11]) compared with a sample signal for the major mass ^{24}Mg of 25 to 30 V.

One hundred carbon and oxygen-isotope speleothem and six hostrock bulk samples were analyzed using a Kiel II carbonate device connected to a ThermoFinnigan MAT 252 Isotope Ratio Mass Spectrometer in the laboratories of the Vrije Universiteit Amsterdam, The Netherlands (Table 1 and Fig. 2; for sampling increments see Fig. 2). Repeated analyses of carbonate standards (GICS, NBS 19 and NBS 18) show an external reproducibility of <0.1‰ for δ^{18}O and <0.05‰ for δ^{13}C. Duplicate samples, run every 10th sample, show scatter of ±0.1‰ or less for both δ^{18}O and δ^{13}C. Per tray of 44 samples, eight standards were measured. The standards used included an in-house calcite standard (GICS) calibrated against SRM NBS 18 and SRM NBS 19. All isotope results are reported in ‰ relative to the V-PDB standard in the conventional manner.

Calcium, Mg, Sr, Mn, and Fe elemental concentrations were established by inductively coupled plasma-atomic emission spectrometry using a Variant Liberty Series II ICP-AES Axial machine in the laboratories of the Vrije Universiteit Amsterdam, The Netherlands (Table 1 and Figs. 2 and 4; for sampling increments see Fig. 2). Element concentrations were calculated applying a five-point calibration curve. Approximately 0.8 to 1 mg of powdered sample was dissolved in 1 N HNO_3 with subsequent dilution to a ~0.1 N HNO_3 solution. The small sample size made accurate measurements of powder weights difficult. Raw solution data were

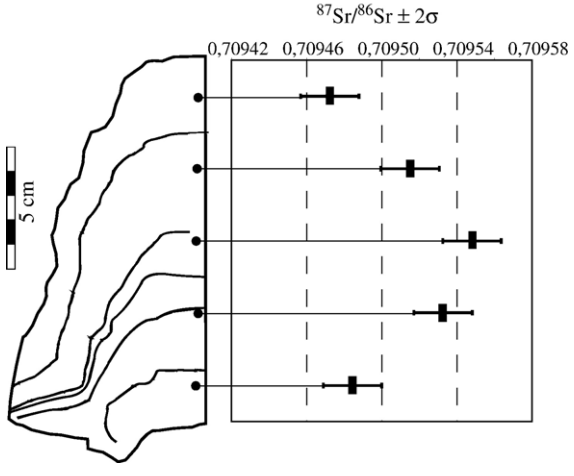

Fig. 5. Strontium-isotope data of Aoufous speleothem. ^{87}Sr/^{86}Sr ratios are plotted against their sampling locality on speleothem. Error bars represent not the individual analytical error of the mass spectrometry but a common error deduced form repeated measurements of the USGS EN-1 measured during the same period.

Table 4
$^{87}Sr/^{86}Sr$ values of the Aoufous speleothem

Sample/standard name or number	$^{87}Sr/^{86}Sr$ measured	$\pm 2\sigma$[a]	$^{87}Sr/^{86}Sr$[b]
NIST NBS 987	0.710238	0.000009	0.710255
pos5	0.709455	0.000009	0.709472
pos20	0.709498	0.000009	0.709515
pos25	0.709531	0.000009	0.709548
Pos33	0.709515	0.000009	0.709532
Pos40	0.709467	0.000009	0.709484
USGS EN-1	0.709157	0.000009	0.709174

[a]Uniform errors representing the reproducibility of USGS EN-1 during the period of sample measurements.
[b]Corrected to USGS EN-1 value stated by McArthur et al. (2001).

converted to elemental ratios by assuming that the sample was stoichiometrically pure calcite. All element data were normalized to a Ca concentration of 40 weight %. Analytical precision of repeated analyses is ±1.5% for Ca and ±8% for Mg, Sr, Mn and Fe. Routinely 10% of all samples were measured as duplicates.

XRD analysis of 12 samples confirmed the assumption of stoichiometrically pure calcite and indicated that all Ca and Mg are present as carbonate-bound cations. For this a Philips MPD diffractometre (quartz internal standard) was used. The Mg content was quantified using the linear displacement of the d(104) reflection between calcite (3.035 Å) and dolomite (2.886 Å). Methods described in detail in Füchtbauer and Richter (1988).

To determine the possible relationship between host rock and stalactite Sr-isotope ratios, five carbonate subsamples were collected along the main speleothem axis and measured in the isotope laboratory of the Ruhr-Universität Bochum, Germany (Fig. 5; Table 4). Sr-isotope ratios were determined using a Finngan MAT 262 mass spectrometer. In order to overcome efficiency differences of individual collectors, all measurements were performed in a so called "dynamic mode" (peak hoping mode). Per sample a minimum of 100 and a maximum of 150 ratios were measured. As an abortion limit for the data collection a relative error (2 standard error (2σ mean)) of 10 ppm was defined. For the year 2006 the average values for the two SRM's measured routinely are 0.710238±0.000038 2σ (n=44) for the NIST NBS 987, and 0.709160±0.000029 2σ (n=35) for the USGS EN-1, respectively. The reproducibility of these two standard reference materials (SRM's) for the period of sample measurements reported in this paper is NBS 987=0.710238±0.000016 2σ (n=4) and USGS EN-1=0.709156±0.000009 2σ (n=4). The samples and the modern biological calcite USGS EN-1 pass through an identical analytical procedure. Therefore the short time reproducibility of the USGS EN-1 mirrors that of sample calcite including Sr separation and mass spectrometry. $^{86}Sr/^{88}Sr$ ratios are normalized to 0.1194.

From pits, drilled parallel to the existing sample sites, approximately 2 mg of carbonate was recovered. The material was dissolved in 2.5 M HCl, centrifuged and subsequently the Sr fraction was separated using 2.5 M HCl to quartz glass columns and BioRad ion exchange resin (AG-50W-x8, 200–400 mesh). The $^{87}Sr/^{86}Sr$-ratios were measured on a Finnigan Mat 262 mass spectrometer.

Cathode luminescence imaging (CL; Fig. 3) was performed using a hot stage (HC1-LM) at the Ruhr-Universität Bochum, Germany (Richter et al., 2003).

4. Results

The speleothem $\delta^{26}Mg$ values along the time-series section vary between −4.39‰±0.02 2σ (sample 17) and −4.17‰±0.05 2σ (sample 30; Table 2). The observed difference of 0.22‰ exceeds the error of the external reproducibility of ±0.03‰ as defined by the 6 samples extracted from the same layer at point 33 (Table 5). A trend to lower δ^{26} Mg values across segments I to III (Fig. 2) is reversed within segment III and followed by an

Table 5
Analytical results of samples taken perpendicular to the speleothem axis (Hendy test)

Sample number	$\delta^{13}C$‰ (VPDB)	$\delta^{18}O$‰ (VPDB)	$\delta^{25}Mg$‰ (DSM3)	$\pm 2\sigma$	$\delta^{26}Mg$‰ (DSM3)	$\pm 2\sigma$
33.0a			−2.19	0.01	−4.22	0.01
33.0b			−2.18	0.01	−4.12	0.03
33.0c			−2.16	0.02	−4.19	0.04
33.0d			−2.18	0.03	−4.21	0.03
33.0e			−2.17	0.02	−4.19	0.03
33.0f			−2.19	0.01	−4.22	0.02
Hendy 1	−1.8	−9.3				
Hendy 2	−1.7	−9.1				
Hendy 3	−1.2	−8.4				
Hendy 4	−5.1	−10.5				
Hendy 5	−2.0	−9.6				
Hendy 6	−2.1	−9.6				
Hendy 7	−2.1	−9.6				
Hendy 8	−2.0	−9.4				
Hendy 9	−2.1	−9.5				
Hendy 10	−2.2	−9.6				
Hendy 11	−2.2	−9.6				
Hendy 12	−2.2	−9.4				
Hendy 13	−2.1	−9.3				
Hendy 14	−2.0	−9.6				
Hendy 15	−2.0	−9.6				
Hendy 16	−1.8	−9.4				
Max	−1.2	−8.4	−2.172		−4.187	
Min	−5.1	−10.5	−2.189		−4.224	
Average	−2.2	−9.5	−2.181		−4.205	
Standard dev.	0.82	0.41	0.007		0.015	

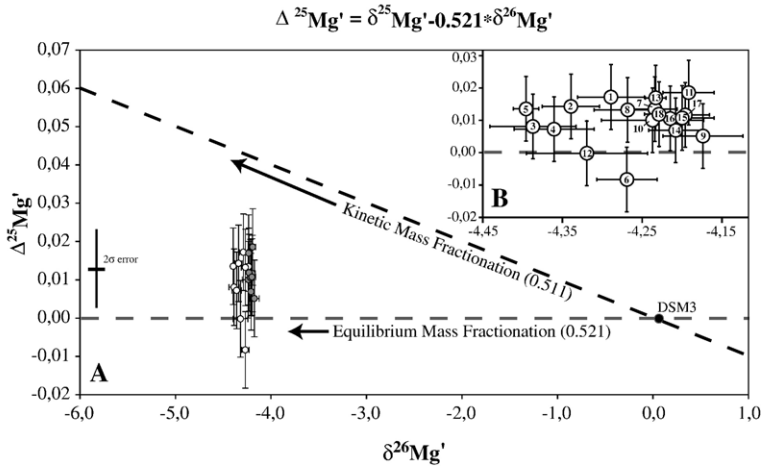

Fig. 6. Three-isotope-plot of Aoufous speleothem Mg-isotope data. A) Three-isotope-plot made linear by the expression $\delta^{25}Mg' = \beta\delta^{26}Mg' - \beta\delta^{26}Mg'_{ref} - \delta^{25}Mg'_{ref}$. Note that the data neither fulfilled the requirements for a pure equilibrium mass fractionation nor for kinetic mass fractionation. B) Enlargement of isotope plot with indication of sample numbers (cf. Fig. 2).

overall trend to higher values is observed into the base of segment V. Segment V is characterized by more or less stable δ^{26}Mg values followed by a renewed shift to a lower value in segment VI (Fig. 2). The values of the Turonian host limestone range from −3.57‰ ± 0.09 2σ to −3.69‰ ± 0.07 2σ (Table 2).

This fractionation pattern is also displayed in the three-isotope-plot (Fig. 6). In a three-isotope-plot the relation between the two pairs of isotopes is defined by an exponential factor β. For easier assessment the three-isotope-plot can be made linear by the expression $\delta^{25}Mg' = \beta\delta^{26}Mg' - \beta\delta^{26}Mg'_{ref} - \delta^{25}Mg'_{ref}$ (Young and Galy, 2004), were the slope represents the exponent β. Therefore all data are plotted in a $\delta^{26}Mg'$–$\delta^{25}Mg'$-diagram. Fig. 6 displays that all data points plot within the 2σ margin along a linear fractionation line with a slope of 0.518 ± 0.12 (2σ). In consequence both δ^{26}Mg and δ^{25}Mg can be used to describe the fraction behaviour of the samples without interference from analytical artefacts.

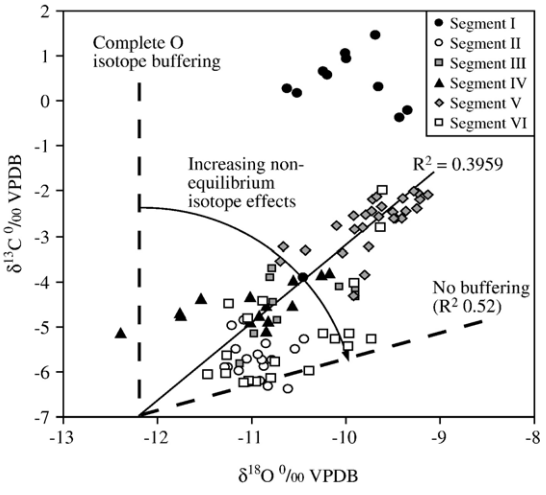

Fig. 7. Non-equilibrium isotope effects on light stable-isotope ratios. Oxygen and carbon-isotope effects of progressive loss HCO_3 during the degassing of CO_2 and resulting calcite precipitation on the isotopic composition of the speleothem (modified from Mickler et al., 2006). Depending on the speleothem interval (I–VI in Fig. 2 and small inset in upper right corner this figure), the Aoufous speleothem data (black dots) were affected by variable degrees of non-equilibrium fractionation.

Whereas the results of the Cambridge1 versus the DSM3 standard solutions measurements document the long-term stability of the mass spectrometer technique, the reliability and robustness of the method is corroborated by what is termed "Hendy-test" for traditional stable isotopes, i.e., the analysis of several time-parallel samples within one growth increment in order to asses the internal variability of the geochemical composition of a given speleothem (Table 5). Six samples from the same layer, drilled parallel to the time-series data set, underwent the complete analytical procedure. All results plot within an error of ±0.030 2σ and ±0.013 2σ for the δ^{26}Mg and δ^{25}Mg, respectively. Possible laboratory artefacts (fractionation, contamination) on the determined delta values from the chemical separation or the mass spectrometry can be ruled out. The test also suggests that the trend along the profile of the dripping stone is geologically significant and must be related to the precipitation of the carbonate.

Speleothem oxygen-isotope data range between −12.4 and −9.1‰ (mean −10.4‰; 1σ = 0.7‰) and

carbon values are between +1.5 and −6.4‰ (mean −3.8‰; 1σ=1.9‰, Table 1 and Figs. 2 and 4). Host rock data ($n=6$) range from −0.9 to +1.8‰ for carbon (mean 0.4‰) from −7.5 to −5.3‰ for oxygen (mean −7.2‰; Fig. 4). For the speleothem data, the overall pattern is a broad co-variance between $\delta^{13}C$ and $\delta^{18}O$, with a shift to lower values in the lower third of the speleothem, followed by a trend towards higher values and a smaller-scale oscillating pattern in the uppermost, youngest portions of the speleothem. Pronounced shifts take place across speleothem growth stops (hiatuses: Fig. 2, gray vertical bars) and are most pronounced in the $\delta^{13}C$ record. With respect to the isotope pattern, several distinct growth regions of this specific speleothem are differentiated and plotted separately in Fig. 7 as carbon and oxygen-isotope data should be analyzed within individual areas of speleothem growth. A tentative first approach is to subdivide the data set into growth intervals I to VI separated by hiatus zones (gray, horizontal bars in Fig. 2).

The outcome of the Hendy test suggests invariant $\delta^{13}C$ and $\delta^{18}O$ data (with the exception of one sample point collected near a small vein; sample "Hendy 4" in Table 5) supporting the assumption of pristine calcite as indicated by the CL imaging. Carbon and oxygen-isotope data from the Turonian host rock range between −9.1 and −5.9‰ for $\delta^{13}C$ and from −9.6 to −8.8‰ for $\delta^{18}O$ (Fig. 4, Table 1).

Speleothem trace-elemental data are below detection limit for Mn. Total Fe elemental compositions range between below detection limit and 200 ppm (Table 1). Strontium ranges between 217 and 1011 ppm (mean 617 ppm; 1σ=198 ppm) and Mg abundances are between 2999 and 9661 ppm (mean 7393 ppm; 1σ=1581 ppm).

Based on optical comparison, an overall first order pattern of lower values in speleothem segments II and III, followed by an overall shift to higher values in segments IV and V, followed by a return to lower values across segment VI characterizes all isotope system and trace element data sets (Fig. 2). The interference of long-scale trends in isotope values and short-term, punctuated events (Fig. 2), however, results in rather poor correlation coefficients between $\delta^{26}Mg$, $\delta^{13}C$, $\delta^{18}O$ and trace elements. For $\delta^{13}C$ and $\delta^{18}O$, the correlation coefficient is moderate (0.629) but a significantly better correlation is found for Mg versus Sr (0.765) and the correlation is lower for $\delta^{26}Mg$ versus Mg_{ppm} (0.445). The correlation coefficient of the magnesium isotope ratios against any of the other proxies is commonly poor ($\delta^{26}Mg$: $\delta^{13}C=0.127$; $\delta^{26}Mg$:$\delta^{18}O=0.267$). It must be noted, however, that the data sets shown for $\delta^{26}Mg$ forms an insufficient basis for any statistical treatment of these data.

Strontium-isotope data ($^{87}Sr/^{86}Sr$) from the Aoufous speleothem range between 0.709548 and 0.709472 (mean 0.709510; Fig. 5). These differences are small but it is significant and important that they do not plot on the Turonian seawater values as expected from the host limestone. The values are low at the base; gradually shift to higher values and back to low values towards the top of the speleothem (Fig. 5; Table 4).

5. Data interpretation and discussion

5.1. Comparison with speleothem data from limestone hostrock caves

Galy et al. (2002) reported on differences of dripping water $\delta^{26}Mg$ values of caves situated in dolostone and limestone hostrocks. Basically, in dolostone caves, there is very little isotopic difference between the host dolomite and the dripping waters when the precipitated mineral is calcite, whereas larger isotopic differences exist when the host rock is calcite (Galy et al., 2002). This implies that in the case of the limestone cave of Aoufous, only the limestone hostrock data of Galy et al. (2002) and Young and Galy (2004) are comparable and should be considered (Table 2). Three of the speleothem data of Galy et al. (2002) range between $\delta^{26}Mg$ ratios of −4.32 and −4.39‰ and overlap with data from the Aoufous speleothem whereas one is considerably higher (−2.8‰) and one is markedly lower (−5.1‰; Table 2).

The hostrock $\delta^{13}C$ and $\delta^{18}O$ data are typical for diagenetically stabilized Cretaceous marine limestones whereas the low $\delta^{18}O$ values of the speleothem reflect the influx of ^{18}O depleted meteoric water (Immenhauser et al., 2007).

5.2. Significance of the hostrock Mg budget

Galy et al. (2002) proposed that in limestone caves, because of the low Mg content of the hostrock, the Mg-isotope composition is more sensitive to external Mg-isotope sources including silicate weathering and processes in the soil zone. Similar conclusions were drawn by Tipper et al. (2006a,b), analyzing the $\delta^{26}Mg$ ratios of the water in small rivers draining limestone hostrock in the French Jura Mountains. This because Mg is often a major constituent of silicate minerals and certainly of dolomite whereas it is only present in traces in low-Mg calcite.

The moderately elevated Mg elemental content of the Aoufous speleothem (up to 9600 ppm Mg or approximately 3 mol% $MgCO_3$; Table 1) is not in concert with the low-Mg calcite composition of the Turonian

hostrock and staining tests of six host rock samples revealed that the carbonate contains no dolomite. This is in agreement with an external source for the elevated Mg elemental composition of the Aoufous stalagmite. Following Galy et al. (2002), a possible source for the excess Mg could be related to airborne dust and dolomites as well as metamorphic and non-metamorphic crystalline basement rocks are exposed in the vicinity of the Aoufous cave locality. The Aoufous data (Fig. 5, Table 4) point to a source high in radiogenic Sr such as siliceous rather than dolomitic material. Banner et al. (1996) reported Saharan dust $^{87}Sr/^{86}Sr$ ratios of between 0.7145 and 0.7168 and Neogene siliciclastics with ranges of 0.7180 to 0.7200. The speleothem $^{87}Sr/^{86}Sr$ values range between 0.709472 ± 0.000009 2σ and 0.709548 ± 0.000009 2σ (normalised to USGS-EN-1 0.709175, McArthur et al., 2001) and thus significantly exceed the average Sr-isotope composition of the Turonian limestone host rock of approximately 0.707348 (McArthur et al., 2001). This pattern is in good agreement with silicates as source for the Mg and Sr and the observed Mg and Sr isotope values and supports the significance or airborne dust and dune material weathering processes atop of the Turonian lime hostrock. XRD analysis of two sand samples, collected in the vicinity of the cave, indicates that the aeolian material contains dolomite as well as plagioclase and kali feldspar hence providing a source for radiogenic Sr.

5.3. Controlling factors of isotope and trace elemental shifts in the Aoufous speleothem

The covariance between different isotope and trace elements systems in speleothems is a characteristic feature of many cave records. For the C and O isotope system, Mickler et al. (2006) suggested that this observation is consistent with non-equilibrium isotope effects but acknowledge the significance of climatic factors causing positive co-variance. In karstic environments, the chemistry of waters is affected by: (1) the chemistry and mineralogy of the local host rock and the regolith; (2) the amount of meteoric precipitation (arid versus humid), the chemistry of the rainwater and its evolution prior to entering the cave system, and the aquifer evolution; and (3) the kinetics and growth rate of the carbonate phase as influenced by temporal variations in PCO_2 in the cave (Frisia et al., 2000).

Each of the geochemical proxies applied in this study is governed by different internal and external factors. In order to asses the co-variance of the three isotope systems and the trace elements, however, an interpretation considering the specific, long-term climatic variability of NW Africa (alternating arid-saharan and humid-monsoonal climate; Rohling et al., 2002; Larrasoaña et al., 2003) is needed. Fig. 8 provides a conceptual model summarizing the main controlling factors in a tentative manner.

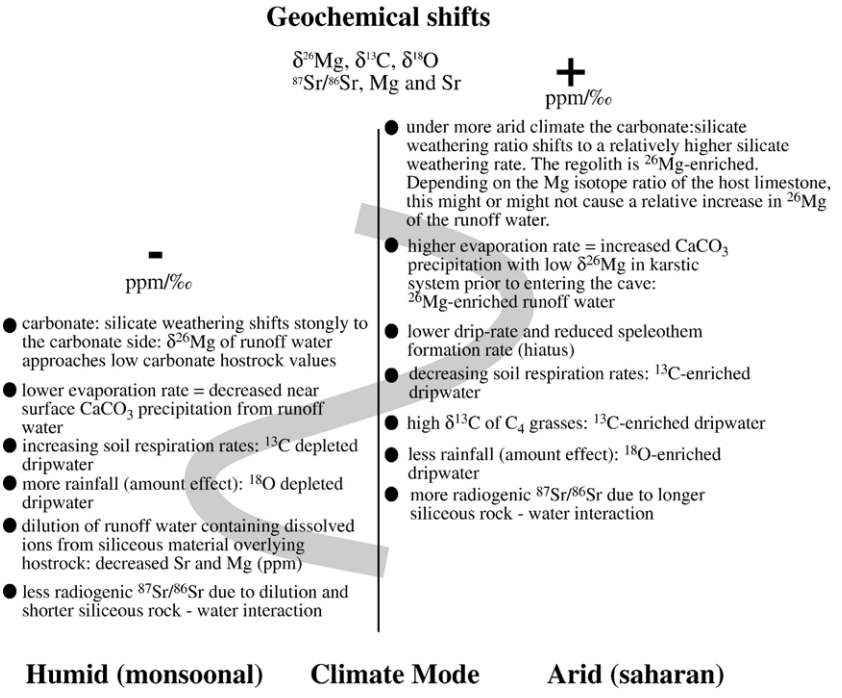

Fig. 8. Conceptual model of environmental factors controlling the isotope and trace element shifts in the Aoufous speleothem of NW Africa.

With respect to the Mg-isotope system the following considerations are of interest: whereas the oxygen-isotope system is strongly affected by exchange between the liquid and the gaseous phase (evaporation; Faure, 1986), no (or only a very minor) change in the Mg-isotope ratio of water is expected during evaporation. In contrast, the evaporation-related, near-surface precipitation of carbonate from meteoric runoff water within the regolith or karstic system prior to entering the cave system is expected to affect speleothem δ^{26}Mg ratios. The precipitated carbonate phase is preferentially enriched in the light isotope by up to 2.5‰ relative to the meteoric runoff water that in turn shifts to higher δ^{26}Mg values (Tipper et al., 2006a). This process goes on during the fractionation between calcitic speleothem and meteoric water in the cave itself (Galy et al., 2002), with speleothem calcite δ^{26}Mg being lower than that of the dripwater (Fig. 8). Two contrasting interpretations are possible: (1) during arid phases, when evaporation and thus near-surface carbonate precipitation (with low δ^{26}Mg) was higher, the dripwater entering the cave was enriched in ^{26}Mg and hence the speleothem δ^{26}Mg shifts to higher values (Figs. 2 and 8). (2) Wetter conditions cause higher carbonate weathering and higher pCO_2 in the karst solutions. As degassing drives calcite precipitation, more near-surface carbonate precipitation took place again causing the dripwater to be enriched in ^{26}Mg. Here, interpretation 1 is favoured for the time being, this because it is in better agreement with data from other isotope systems and results of elemental analysis. Nevertheless, neither of the two possibilities can at present be confirmed. This as data from soil and karst-zone carbonates and the resulting dripwater (cave monitoring) are required to asses the significance of the individual factors. This is the topic of further work.

Magnesium ions in meteoric runoff waters are predominantly derived from the weathering of carbonates and to a lesser degree of (less soluble) silicate minerals of the continental crust (Meybeck, 1987; Tipper et al., 2006a). Particularly, silicate weathering fractionates Mg-isotope ratios with the heavy Mg retained in the soil and depleted runoff waters. This implies that δ^{26} Mg values in speleothems will tend to lower values during more arid periods when the silicate weathering is more intense (but still minor compared to the carbonate weathering rate) due to longer water rock interaction periods, and higher values characterized dry intervals with reduced regolith weathering (Tipper et al., 2006b). Shorter residence time of groundwater during monsoonal phases preferentially weathers carbonate whereas silicates are less affected (Tipper et al., 2006a, b). This predicts that the balance for the Mg-isotope composition might shift strongly towards limestone-derived Mg having depleted Mg-isotope values (between −3.69 and −3.57‰ δ^{26}Mg; Table 2).

The above interpretation is well in agreement with slightly less radiogenic $^{87}Sr/^{86}Sr$ during monsoonal phases resulting from the dilution effect and lower residence time of runoff water in the regolith. Similarly, Sr and Mg abundances are decreasing due to a dilution of the dissolved ions and selective leaching of trace elements from soils (Fairchild et al., 2000, 2001; Huang et al., 2001). In contrast, slightly more radiogenic $^{87}Sr/^{86}Sr$ is incorporated in the spelean calcite during arid periods due to increased silicate weathering rates in the regolith. If the before considerations hold true, then higher Sr and Mg elemental values are correlated with dryer and lower Sr and Mg elemental values with more humid periods (Fig. 8).

Strontium incorporation is also dependent on precipitation rate, in this case mainly controlled by temporal variations in PCO_2 in the cave and the amount of drip water entering the cave. Since Sr and Mg positively correlate in the stalagmite a crystallographic effect can be ruled out. Experimental studies of Sr partitioning on marine analogue solutions show a weak dependence on precipitation rate with K_{Sr} increasing around 15% as precipitation rates increase by an order of magnitude (Fairchild et al., 2000, 2001).

The C-isotope system is controlled by the isotopic composition of the host carbonate, representing the main reservoir, but also the amount of soil-zone CO_2 entering the system. The soil-zone activity is determined by the climate and the vegetation cover (C3 versus C4 plants; Baker et al., 1997). All of these considerations are in agreement with the isotopic trends observed in the Aoufous speleothem but should be considered as a first working hypothesis for the time being (Fig. 8).

5.4. Kinetic versus equilibrium precipitation

According to Galy et al. (2002) the temperature dependence of the δ^{26}Mg isotope fractionation between 4 and 18 °C, the common temperature range of many caves, is less than 0.02‰/AMU/°C. The Aoufous speleothem spread of 0.22‰ between δ^{26}Mg maxima and minima would require centuries to millennia-scale temperature changes in excess of 10 °C within the cave system. A long-term change in annual mean air temperature in the order of 10 °C has been reconstructed for Pleistocene speleothem growth changing from glacial to interglacial conditions in Western and Central Europe (Baker et al., 1995; Genty et al., 2003; Niggemann et al., 2003). In contrast, millennia-scale temperature changes of more

than a few degrees Celsius are not in agreement with climate model data for the Pleistocene of NW Africa. Due to changes in insolation, the Mid-Holocene "green Sahara" episode for example, one of the largest climatic anomalies of the last 12 Kyr, was characterized by cooler tropical and subtropical winter paleo-temperatures. Nevertheless, these changes were in the order of 1.5 °C only and present-day annual temperature changes are in the order of 5 °C and less (de Noblet-Decoudre et al., 2000; Braconnot et al., 2002). This implies that the cyclical variation in the Mg-isotopic composition of the speleothem is probably not explained by temperature-dependent fractionation effects in the cave system due to long-term climate warming or cooling.

The δ^{26}Mg versus the δ^{25}Mg data plot along a linear regression line with a slope of 0.518±0.012 2σ. Consequently, these data lie within the area defined by the slopes of 0.511 and 0.521 representing an isotope fraction according to a kinetic and equilibrium fractionation law (Fig. 6). Considering the analytical error, it becomes obvious that a purely kinetic or equilibrium fractionation process cannot be responsible for the observed isotope pattern. According to a simple mixing model a slope of 0.518 would represent an approximately 80% equilibrium dominated fractionation. In a Δ^{25}Mg′ versus δ^{26}Mg′ plot that magnifies the difference – difficult to observe in traditional three-isotope-plot – 16 out of 18 data fall in the area bounded by the kinetic and equilibrium fractionation line, which is accessible by either a single stage fractionation, or two subsequent stages of kinetic and equilibrium fractionation (Fig. 6; Galy et al., 2002; Young and Galy, 2004). Only two samples would require a multi-stage fractionation. Nevertheless, assuming a 2σ error of ±0.01‰ for Δ^{25}Mg′, these data should be considered to be non-significant. It must be kept in mind, however, that the slopes shown in Fig. 6 are calculated for the pure ionic forms of Mg. We are aware of the fact that this is probably an oversimplification of the processes taking place during precipitation of the carbonate. It is not well understood how Mg enters the cave system: in its ionic form, as an aquacomplex, or as organic/inorganic compound.

5.5. Strengths and weaknesses of this study and implications for speleothem research

A clear strength of the present study is the detailed geochemical data set within a single, well-preserved calcitic speleothem. This allows for: (i) the direct comparison of the Mg-isotope time-series data set with several other geochemical proxies reflecting environmental change in a continental setting and (ii) for a tentative discussion of the controlling factors. Nevertheless, an improved understanding of the complex fractionation paths of the Mg-isotope system in speleothem calcite requires access to coeval authigenic carbonates and water samples. This is not the case here and a weakness of this study. Furthermore, the unspecified age (>500 kyr) limits the possibilities of data comparison with other studies.

The present paper follows in part previous work by Galy et al. (2002). Given the lack of published Mg-isotope data from limestone caves in general and specifically of times-series, the results of this study are considered to be meaningful for speleothem-based climate studies. Assuming that the considerations outlined herein are correct, the Mg-isotope proxy bears important information concerning shifts in alternating arid and humid continental climate systems such as NW Africa.

6. Conclusions

The following conclusions can be drawn from the geochemical analysis of the Pleistocene Aoufous speleothem:

(1) The first order pattern of speleothem time series analyses of δ^{26}Mg isotopes is positively correlated with δ^{18}O, δ^{13}C, ^{87}Sr/^{86}Sr and Sr and Mg element concentration data. The difference of 0.22‰ in δ^{26} Mg is significantly beyond the error of the external reproducibility of ±0.03‰ for δ^{26} Mg. In some short sections of the record oxygen or carbon isotopes are negatively correlated with for instance δ^{26}Mg. This points to higher order factors overriding the large scale trends.
(2) The low temperature dependence of the δ^{26}Mg isotope fractionation and the overall moderate temperature changes in NW Africa between monsoonal and arid phases suggest that long-term temperature changes in the cave where not a main driver of shifts in the spelean calcite δ^{26}Mg.
(3) Under alternating monsoonal and dry climatic conditions, δ^{18}O and δ^{13}C ratios of the Aoufous speleothem are perhaps best interpreted in terms of temperature, rain mass amounts effects and soil respiration rates. Based on out present knowledge, it seems that these factors are not affecting the δ^{26}Mg isotope ratios significantly.
(4) The tentative interpretation of the speleothem δ^{26}Mg ratios derives from the Mg fractionation pattern of mainly carbonate hostrock, and to a lesser degree of silicates, and the evaporation-related precipitation of calcite in the regolith. Increased precipitation rates of carbonates in the

regolith results in a ^{26}Mg-enriched drip-water entering the cave. Increased silicate weathering, due to long groundwater residence time, results in ^{26}Mg-depleted runoff water. In contrast, more rainfall and shorter groundwater residence times enhances carbonate weathering and shifts the δ^{26}Mg ratio towards that of the carbonate hostrock (high or low). These considerations are supported by $^{87}Sr/^{86}Sr$ data of the speleothem calcite.

(5) In order to firmly establish the new δ^{26}Mg proxy in continental palaeoclimate research future work must focus on actively growing speleothems in cave settings that provide access to soil, rainwater, groundwater and dripwater samples as well as to cave temperature monitoring.

Acknowledgements

We acknowledge constructive comments by Dr. E. Tipper, Cambridge and Dr. M. Dietzel, Graz. Speleothem U–Th analysis was performed by Dr. J. Fietzke, IFM-GEOMAR, Kiel. Constructive comments by editor S.L. Goldstein and two anonymous referees are highly appreciated. B. Gehnen, Bochum, is acknowledged for the analysis of the host rock carbon and oxygen isotope data.

References

Baker, A.P., Smart, L., Edwards, R.L., 1995. Palaeoclimate implications of mass spectrometric dating of a British flowstone. Geology 23, 309–312.

Baker, A., Ito, E., Smart, P.L., McEwan, R.F., 1997. Elevated and variable values of ^{13}C in speleothems in a British cave system. Chem. Geol. 136, 263–270.

Banner, J., Musgrove, M.-L., Asmerom, Y., Edwards, R.L., Hoff, J.A., 1996. High-resolution temporal record of Holocene ground-water chemistry: tracing links between climate and hydrology. Geology 24, 1049–1053.

Braconnot, P., Lutre, M.-F., Dong, B., Joussaume, S., Valdes, P., PIMIP participating groups, 2002. How the simulated change in monsoon at 6 ka BP is related to the simulation of the modern climate: results from the Paleoclimate Modeling Intercomparison Project. Clim. Dyn. 19, 107–121.

Chang, V.T.-C., Williams, R., Maskisima, A., Belshawl, N.S., O'Nions, R.K., 2004. Mg and Ca isotope fractionation during $CaCO_3$ biomineralization. Biochem. Biophys. Res. Commun. 323, 79–85.

de Noblet-Ducoudré, N., Claussen, M., Prentice, C., 2000. Mid-Holocene greening of the Sahara: first results of the GAIM 6000 year BP experiment with two asynchronously coupled atmosphere/biome models. Clim. Dyn. 16, 643–659.

de Villiers, S., Dickson, J.A.D., Ellam, R.M., 2005. The composition of the continental river weathering flux deduced from seawater Mg isotopes. Chem. Geol. 216, 133–142.

Dettman, D.L., Lohman, K.C., 1995. Microsampling carbonates for stable isotope and minor element analysis. Physical separation of samples on 20 μm scale. J. Sediment. Res., Sect. A Sediment. Pet. Proc. 65, 566–569.

Fairchild, I.J., Borsato, A., Tooth, A.F., Frisia, S., Hawkesworth, C.J., Huang, Y.-M., McDermott, F., Spiro, B., 2000. Controls on trace element (Sr–Mg) compositions of carbonate cave waters: implications of speleothem climatic records. Chem. Geol. 166, 255–269.

Fairchild, I.J., Baker, A., Borsato, A., Frisia, S., Hinton, R.W., McDermott, F., Tooth, A.F., 2001. Annual to sub-annual resolution of multiple trace-element trends in speleothems. J. Geol. Soc. (Lond.) 158, 831–841.

Faure, G., 1986. Principles of Isotope Geology. John Wiley, New York. 589 pp.

Fleitmann, D., Burns, S.J., Mudelsee, M., Neff, U., Kramers, J., Mangini, A.N., Matter, A., 2003a. Holocene forcing of the Indian monsoon recorded in a stalagmite from Southern Oman. Science 300, 1737–1739.

Frisia, S., Borsato, A., Farichild, I.J., McDermott, F., 2000. Calcite fabrics, growth mechanisms, and environments of formation in speleothems from the Italian Alps and southwestern Ireland. J. Sediment. Res. 70, 1183–1196.

Füchtbauer, H., Richter, D.K., 1988. Sedimente und Sedimentgesteine. In: Füchtbauer, H. (Ed.), Karbonatgesteine. Schweizerbart, Stuttgart, pp. 233–434.

Galy, A., Belshaw, N.S., Halicz, L., O'Nions, R.K., 2001. High-precision measurements of magnesium isotopes by multiple-collector inductively coupled plasma mass spectrometry. Int. J. Mass Spectrom. 208, 89–98.

Galy, A., Bar-Matthews, M., Halicz, L., O'Nions, R.K., 2002. Mg isotopic composition of carbonate: insight from Speleothem formation. Earth Planet. Sci. Lett. 201, 105–115.

Galy, A., Yoffe, O., Janney, P.E., Williams, R.W., Cloquet, Ch., Alard, O., Halicz, L., Wadhwa, W., Hutcheon, I.D., Ramon, E., Carignan, J., 2003. Magnesium isotope heterogeneity of the isotope standard SRM 980 and new reference materials for magnesium-isotope-ratio measurements. J. Anal. At. Spectrom. 18, 1352–1356.

Genty, D.D., Blamart, R., Ouahdi, M., Gilmour, A., Baker, J., Jouzel, S., Van-Exter, 2003. Precise dating of Dansgaard-Oeschger climate oscillations in western Europe from stalagmite data. Nature 421, 833–837.

Hendy, E., 1971. The isotopic geochemistry of speleothems-I. The calculation of the effects of different modes of formation on the isotopic composition of speleothems and their applicability as paleoclimate indicators. Geochim. Cosmochim. Acta 35, 801–824.

Huang, Y.-M., Fairchild, I.J., Borsato, A., Frisia, S., Cassidy, N.J., McDermott, F., Hawkesworth, C.J., 2001. Seasonal variations in Sr, Mg, and P in modern speleothems (Grotta di Ernesto, Italy). Chem. Geol. 175, 429–446.

Immenhauser, A., Dublyansky, Y.V., Verwer, K., Fleitman, D., Pashenko, S.E., 2007. Textural, elemental and isotopic characteristics of Pleistocene phreatic cave deposits (Jabal Madar, Oman). J. Sediment. Res. 77, 68–88.

Larrasoaña, J.C., Roberts, A.P., Rohling, E.J., Winklhofer, M., Wehausen, R., 2003. Three million years of monsoon variability over the northern Sahara. Clim. Dyn. 21, 689–698.

Meybeck, M., 1987. Global chemical weathering of surficial rocks estimated from river dissolved load. Am. J. Sci. 287, 401–428.

Mickler, P.J., Libby, A.S., Banner, J.L., 2006. Large kinetic isotope effects in modern speleothems. GSA Bull. 118, 65–81.

McArthur, J.M., Howarth, R.J., Bailey, T.R., 2001. Strontium isotope stratigraphy: lowess version 3. Best-fit to the marine Sr-isotope curve for 0 to 509 Ma and accompanying look-up table for deriving numerical age. J. Geol. 109, 155–170.

Neuser, R.D., Richter, D.K., 2007. Non-marine radiaxial fibrous calcites — examples of speleothems proved by electron backscatter diffraction. Sed. Geol. 194, 147–154.

Niggemann, S., Mangini, A., Richter, D.K., Wurth, G., 2003. A paleoclimate record of the last 17,600 years in stalagmites from the B7 cave, Sauerland, Germany. Q. Sci. Rev. 22, 555–567.

Richter, D.K., Götte, T., Niggemann, S., Werth, G., 2002. Cathodoluminescence of carbonate speleothems: state of the art. In: Carrasca, F., Duran, J.J., Andreo, B. (Eds.), Karst and Environment. Fundacion Cueva de Nerja, Malaga, pp. 381–387.

Richter, D.K., Götte, T., Götze, J., Neuser, R.D., 2003. Progress in application of cathodoluminescence (CL) in sedimentary petrology. Min. Pet. 79, 127–166.

Rohling, E.J., Cane, T.R., Cooke, S., Sprovieri, M., Bouloubassi, I., Emeis, K.C., Schiebel, R., Kroon, D., Jorissen, F.J., Lorre, A., Kemp, A.E.S., 2002. African monsoon variability during the previous interglacial maximum, Earth Planet. Sci. Lett. 202, 61–75.

Spötl, C., Mangini, A., Frank, N., Eichstädter, R., Burns, S.J., 2002. Start of the last interglacial period at 135 ka: evidence from a high Alpine speleothem. Geology 30, 815–818 (ln. 825).

Tipper, E.T., Galy, A., Bickle, M.J., 2006a. Riverine evidence for a fractionated reservoir of Ca and Mg on the continents: implications for the oceanic Ca cycle. Earth Planet. Sci. Lett. 247, 267–279.

Tipper, E.T., Galy, A., Gaillardet, J., Bickle, M.J., Elderfield, H., Carder, E.A., 2006b. The magnesium isotope budget of the modern ocean: constraints from riverine magnesium isotope ratios. Earth Planet. Sci. Lett. 250, 241–253.

White, W.B., 2004. Paleoclimate records from speleothems in limestone caves. In: Sasowasky, I.D., Mylroie, J. (Eds.), Studies of cave sediments. Kluwer, New York, pp. 135–176.

Young, E.D., Galy, A., 2004. The isotope geochemistry and cosmochemistry of magnesium. Rev. Min. Cosmochem. 55, 197–230.